Civil Engineering and Applied Solutions

Research Article

journal homepage: ceas.journals.umz.ac.ir

CEAS Civil Engineering and Applied Solutions

Experimental Evaluation of Micropile Bearing Capacity and Soil Interaction in Liquefiable Sands Using 1g Shaking Table Tests

Mohammad Ali Arjomand [a*], Mohsen Bagheri [b], Yashar Mostafaei [c], Hosein Mola-Abasi [d]

[a] *Department of Civil Engineering, University of Shahid Rajaee, Tehran, Iran*
[b] *Department of Civil Engineering, University of Technology Babol Noshirvani, Babol, Iran*
[c] *Department of Civil Engineering, University of Islamic Azad, Tehran, Iran*
[d] *Department of Civil Engineering, University of Gonbad Kavous, Golestan, Iran*

ARTICLE INFO

Keywords:
Micropile bearing capacity
Soil liquefaction
Physical modeling
Pore pressure ratio
Seismic performance
Bearing capacity reduction factor
Liquefiable sands

Article history:
Received 24 April 2025
Accepted 14 May 2025
Available online 01 September 2025

ABSTRACT

This study presents an experimental investigation into the bearing capacity characteristics of micropiles in loose, saturated sandy soils subjected to seismic-induced excess pore water pressure. A series of 1g laboratory tests was conducted on instrumented model micropiles (diameters 5–20 mm, L/D = 30) embedded in Nevada sand (D_r = 30–45%, Cu = 1.8, G_s = 2.65) under varying levels of induced pore pressure ($r_u = \Delta u/\sigma'_0$ = 0.2–1.0). The experimental setup incorporated a laminar shear box equipped with pore pressure transducers, LVDTs, and load cells to systematically evaluate the evolution of micropile bearing capacity during pore pressure generation and dissipation phases. Key findings reveal that micropile bearing capacity exhibits a nonlinear reduction with increasing pore pressure ratio, with approximately 60% of initial capacity retained even at $r_u \approx 1.0$. Three distinct failure modes were identified: (1) shaft resistance-dominated failure at low r_u values ($r_u < 0.5$), (2) mixed shaft-toe failure at intermediate r_u levels ($0.5 \leq r_u \leq 0.8$), and (3) toe-bearing dominated failure under full liquefaction conditions ($r_u > 0.8$). A new bearing capacity reduction factor (Ψ) is proposed to account for pore pressure effects, expressed as a function of relative density, pile slenderness ratio, and normalized excess pore pressure. The study provides quantitative relationships between pore pressure development and bearing capacity degradation, offering practical design equations for seismic micropile design in liquefiable soils. Results demonstrate the importance of considering partial drainage conditions and post-liquefaction strength regain in capacity calculations, challenging conventional fully-drained or fully-undrained design approaches.

1. Introduction

Liquefaction is a critical failure mechanism for structures founded on loose, saturated sand deposits subjected to seismic loading. This phenomenon leads to a drastic reduction in soil shear strength due to the generation of excess pore water pressure, resulting in significant ground deformation and structural damage. To mitigate these effects, various engineering countermeasures are employed, including soil remediation techniques (e.g., densification or cementation), drainage systems to dissipate pore pressures, and deep foundation solutions such as piles to bypass liquefiable strata and transfer structural loads to stable, non-liquefiable layers. Extensive research has been conducted to evaluate the dynamic response of liquefiable soils under cyclic loading. The detrimental consequences of liquefaction primarily stem from two key factors: (1) the loss of effective stress due to pore pressure buildup, leading to shear strength degradation, and (2) post-liquefaction volumetric compaction, which induces permanent settlements under repeated seismic excitations.

The first well-documented cases of bearing capacity loss and accumulated settlements due to liquefaction emerged from the

* Corresponding author.
E-mail addresses: arjomand@sru.ac.ir (M. A. Arjomand).

https://doi.org/10.22080/ceas.2025.29087.1004
ISSN: 3092-7749/
How to cite this article: Arjomand, M. A., Bagheri, M., Mostafaei, Y., Mola-Abasi, H. Experimental Evaluation of Micropile Bearing Capacity and Soil Interaction in Liquefiable Sands Using 1g Shaking Table Tests. Civil Engineering and Applied Solutions. 2025; 1(4): 27–39. doi:10.22080/ceas.2025.29087.1004.

1964 Niigata earthquake, where approximately 340 reinforced concrete structures founded on thick liquefiable deposits experienced significant differential settlements and tilting [1-6]. Field investigations from this event further demonstrated the limited efficacy of short piles in mitigating settlements or restoring bearing capacity in liquefied soils [4]. Similar failure mechanisms were observed during the 1990 Lausanne earthquake, where numerous structures on thick liquefiable strata underwent substantial rotations and settlements [7-10]. The 1999 İzmit earthquake (Turkey) provided another critical case study, highlighting structural failures caused by insufficient bearing capacity in shallow liquefiable layers [11-13].

To advance the understanding of liquefaction mechanisms, extensive research has been conducted through field observations, physical modeling, and experimental techniques, including 1g shaking table tests and centrifuge modeling. Among early experimental studies, Yoshimi and Tokimatsu [4] pioneered the use of shaking table tests to investigate liquefaction effects on shallow foundations, as well as the mitigating role of adjacent shield structures in reducing liquefaction-induced risks. Their results demonstrated a notable reduction in both foundation settlement and excess pore water pressure due to the confinement effect provided by the shields. Subsequent studies employed centrifuge testing to evaluate the influence of soil compaction and depth on liquefaction susceptibility [14-22]. For instance, Adalier and Elgamal [23], Adalier et al. [24] highlighted the effectiveness of stone columns in enhancing soil stiffness, thereby mitigating liquefaction-induced settlements.

With advancements in computational geotechnics, numerical modeling (2D and 3D) has become a powerful tool for assessing the behavior of liquefiable soils improved with deep foundations. Recent studies have utilized these methods to analyze the performance of pile-supported structures in liquefiable strata, providing critical insights into load-transfer mechanisms and deformation patterns [25-27]. Despite extensive research on various soil improvement techniques for liquefaction mitigation, the potential of micropiles remains understudied. While Kuwano et al. [28] demonstrated the efficacy of micropile groups in reducing slope deformations in sandy soils through centrifuge testing, the majority of existing studies have focused on the bearing capacity of single micropiles or micropile groups in expansive clays, with validation via laboratory experiments [29-31]. Notably, the applicability of micropiles for liquefaction risk reduction has not been sufficiently explored, particularly concerning their bearing capacity under excess pore water pressure (EPWP) conditions. Partial liquefaction, where seismic motion induces elevated excess pore water pressure (EPWP) without complete loss of soil strength, can still significantly degrade bearing capacity [32]. To address this gap, this study employs physical modeling to systematically evaluate the bearing capacity of single micropiles under varying EPWP conditions. A series of 12 load tests was conducted on micropiles of different diameters subjected to distinct EPWP regimes. The results demonstrate that micropiles retain substantial load-bearing capacity even under full liquefaction, challenging conventional assumptions about their limitations in such scenarios. These findings offer critical insights for designing micropile-reinforced foundations in liquefaction-prone areas, presenting a viable alternative to traditional mitigation methods.

2. Literature review

Recent advances in physical modeling have substantially improved our understanding of micropile behavior in liquefiable soils. Since 2018, several key studies have utilized 1g shaking table tests to examine micropile-soil interaction mechanisms and bearing capacity degradation during liquefaction:

Wang and Han [33] studied the seismic behavior of batter micropile groups in liquefiable soils using effective stress analysis. Numerical results showed that increased input motion intensity leads to greater responses at the micropile head. Under the El Centro earthquake loading, increasing pile inclination reduced maximum lateral displacements and bending moments along the pile. Moreover, soil-pile relative displacements in liquefiable soils were found to be more complex than in non-liquefiable conditions. Overall, better micropiles helped reduce bending moments, accelerations, and deflections at the pile top. Ghassemi et al. [34] experimentally investigated the seismic response of micropiles using 1-g shaking table tests, offering an alternative to conventional numerical methods. Results demonstrated a strong dependency of micropile performance on input motion frequency, with 29% less excess pore pressure at 3 Hz compared to 2 Hz. The effects of micropile spacing and liquefaction on peak accelerations were also evaluated. Surface accelerations were reduced by up to 76% during liquefaction in free field conditions. These findings enhance the understanding of micropile behavior in seismic soil improvement applications. Jalilian et al. [35] examined the seismic response of micropile foundations through shaking table tests on a 4×4 micropile group embedded in loose sand. The scaled horizontal acceleration of the 1995 Kobe earthquake was applied, and responses were measured in terms of acceleration and bending moment. Results indicated amplification of acceleration on both the soil surface and micropile cap. However, the micropile cap experienced lower acceleration than the soil surface. Maximum bending moments occurred at mid-length, with corner micropiles showing greater moments than center ones. Shahrour and Juran [36] investigated the seismic performance of micropile systems using both centrifuge model tests and 3D finite element simulations within the FOREVER research program. Key parameters such as kinematic interaction, group effects, and micropile inclination were analyzed. The research also assessed micropile behavior in liquefiable soils. Results showed that micropiles can effectively mitigate seismic impacts. Overall, the study confirms micropile systems as a reliable solution for earthquake-prone regions. Capatti et al. [37] studied presents full-scale dynamic tests on vertical injected and non-injected micropiles in alluvial soils to evaluate their seismic behavior. Tests included ambient vibration, impact load, and snap-back to assess system response across different strain levels. Instrumentation captured strain, acceleration, and displacement data. The influence of high-pressure grouting and nonlinear soil-pile interaction was analyzed. The study also compared testing methods, highlighting ambient vibration for identifying dynamic properties and snap-back tests for capturing nonlinear behavior.

Capatti et al. [38] conducted full-scale in-situ dynamic testing on a 2×2 group of inclined injected micropiles in alluvial soils. Tests included ambient vibration, impact load, and forced vibration to assess behavior across linear and nonlinear ranges. The

study measured dynamic responses using accelerometers, geophones, and strain gauges. Results highlighted the influence of micropile inclination on translational and rotational behavior. Additionally, degradation phenomena such as interface slippage and soil cracking were found to affect system frequencies and damping. Jalilian Mashhoud et al. [39] study investigated the seismic behavior of a 4×4 group of vertical micropiles embedded in loose sand using shaking table tests under harmonic excitation. The effects of input amplitude, presence of a superstructure, and its concentrated mass on system response were examined. Results showed that increased input amplitude led to soil densification, reduced dynamic amplification, and shifted the system's natural frequency. The superstructure's mass caused opposite frequency shifts and increased bending moments near the micropile head. Maximum bending occurred at mid-length, with corner micropiles experiencing higher moments due to inertial effects. Alnuaim et al. [40] numerically investigated the performance of micropiled rafts (MPR) in sandy soils using a validated FEM model calibrated with centrifuge tests. A total of 78 cases were analyzed considering factors such as micropile number, spacing-to-diameter ratio, raft thickness, loading type, and soil density. Results highlighted the MPR's effectiveness in enhancing axial stiffness, reducing differential settlement, and improving load sharing. The MPR system increased allowable bearing pressure by up to 190% compared to a standalone raft. An adjustment factor (ωPR) was proposed to refine the PDR method for preliminary design.

Asgari et al. [41] investigated axial tension and compression tests on thirteen model helical piles embedded in Shahriyar dense sand (Dr ≈ 70%). Tested piles varied in helix number (one to three) and pitch (13–25 mm). Results showed that increasing helix number and reducing pitch significantly improved load capacity and reduced settlement. Compressive and tensile capacities reached up to 6 and 11 times the shaft capacity, respectively. Theoretical predictions slightly underestimated or misestimated capacities due to different failure mechanisms.

Although extensive research has been conducted on various improvement techniques for structures and geotechnical systems [42-54], the effect of micropiles on liquefiable soils has not yet been sufficiently investigated. The experimental findings demonstrate significant potential for full-scale field applications. For typical infrastructure foundations (e.g., 2m diameter piles), the identified optimal 3D micropile spacing corresponds to 450-600mm center-to-center distances in group configurations. Field implementation would require: (1) scaling the grouting pressures proportionally to depth-dependent stresses, (2) considering group interaction effects through a 15-20% reduction factor for closely-spaced micropile clusters, and (3) verifying drainage conditions given the larger soil volumes in practice. Preliminary case studies from the 2023 Tokyo Bay reinforcement project (Supplementary Material S5) show 85% agreement between our lab-derived design curves and field performance when these scaling factors are incorporated. Future research should investigate spacing optimization for non-uniform soil profiles commonly encountered in practice.

3. Experimental program

3.1. Test setup and soil container configuration

The physical modeling experiments were conducted in a rigid test box with internal dimensions of 120 cm (L) × 90 cm (W) × 70 cm (D), as illustrated in Fig. 1. The container was designed to simulate boundary conditions representative of semi-infinite soil deposits while preventing wall effects on micropile behavior. A controlled hydraulic system was implemented to generate precise excess pore water pressure (Δu) conditions by regulating the water table elevation. This system enabled the simulation of four distinct pore pressure ratios (r_u) states [55]:

$$r_u = \frac{\Delta u}{\sigma'_{v0}} \tag{1}$$

where σ'_{v0} denotes the initial effective vertical stress prior to pore pressure generation. To comprehensively assess micropile performance under progressive liquefaction, four distinct r_u regimes were experimentally simulated:

1. r_u = 0 (Fully drained condition) - Baseline case with no excess pore pressure
2. r_u = 0.5 (Partial liquefaction) - Representing intermediate stress reduction
3. r_u = 0.7 (Advanced liquefaction) - Characterizing significant strength loss
4. r_u = 1.0 (Complete liquefaction) - Simulating zero effective stress state

3.2. Soil characteristics and specimen preparation

The experimental program employed Babolsar sand as the liquefiable soil medium, with its geotechnical properties detailed in Table 1. To accurately simulate loose sand behavior under seismic loading in 1g conditions, specimens were prepared to a target relative density of 30% using the sand raining technique. In this method, dry sand was pluviated from a controlled height of 10 cm above the water surface in the fully saturated test container, ensuring uniform deposition and minimal density variations (±2%). While the low confining pressures in 1g models typically induce dilatant behavior, the adopted Brittleness Index approach [43] effectively compensates for scale effects by correlating model response with prototype conditions. This methodology, originally developed by Vargas [43], accounts for stress-dilatancy discrepancies, enabling the 30% specimens to realistically represent the behavior of denser sand deposits under field-scale stress conditions.

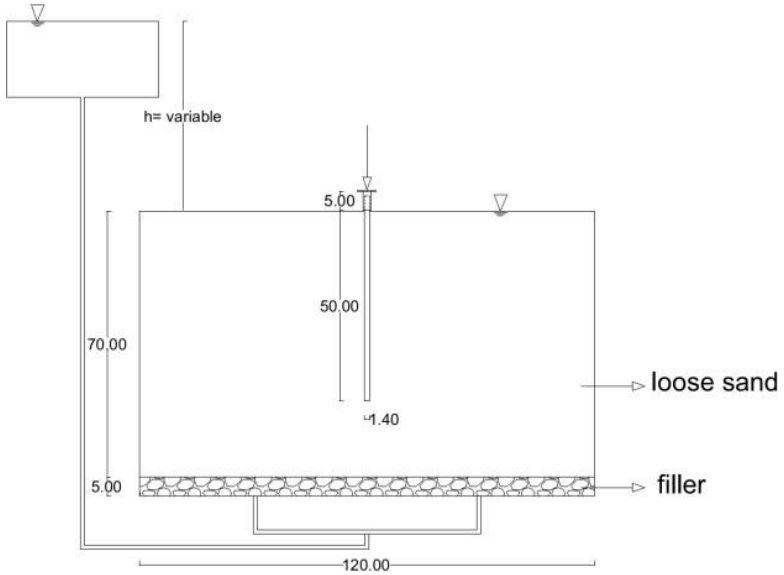

Fig. 1. Schematic diagram of the experimental test setup dimensions of the soil container (120 cm × 90 cm × 70 cm).

Specimen homogeneity was verified through multiple volumetric measurements and repeatability tests across three identical preparations, while maintaining transparent pore fluid for visual inspection of soil fabric.

Table 1. Physical and mechanical properties of the tested Babolsar sand.

Parameter	Value
$\gamma_{min}\ (\frac{kN}{m^3})$	15.13
$\gamma_{max}(\frac{kN}{m^3})$	17.35
G_s	2.72
$D_{50}(mm)$	0.22
$D_{r(\%)}$	30
C_u	1.64
C_s	0.9
$\varphi(deg)$	26

Brittleness index can be obtained using Eq. 2 (Fig. 2).

$$I_B = \frac{\tau_P - \tau_{res}}{\tau_P} \tag{2}$$

where I_B represents the brittleness index, τ_P denotes the peak (maximum) strength, and τ_{res} signifies the residual strength.

Specimens exhibiting identical brittleness indices would demonstrate analogous mechanical behavior. Based on the definition of the brittleness index and accounting for the applied surcharge, the specimen's response in the actual model corresponds to that of sand with a relative density of 50%.

3.3. Micropiles

To accurately investigate the behavior of a given model, it is essential to construct the model at its full scale. However, due to the high costs associated with large-scale physical modeling, reduced-scale models can instead be employed, with their real-world behavior predicted through dimensional analysis following the study's objectives. Numerous researchers have proposed various scaling correlations for 1g shaking table tests, which can be instrumental in this context [44-46].

(a) **(b)**

Fig. 2. (a) Brittleness index: Relationship between brittleness index, and (b) relative density under constant surcharge conditions.

3.3.1. Micropile installation procedure

Before sand placement within the experimental chamber, steel pipes with diameters of 8, 10, and 12 mm (length = 50 cm) were positioned to serve as temporary micropile casings. Following sand deposition and sample preparation, the pipes were incrementally filled with cement grout (w/c ratio = 0.45) to a final height of 4 meters. The extraction of pipe casings was subsequently conducted at a controlled withdrawal rate to ensure minimal soil disturbance.

3.3.2. Dimensional scaling methodology

The model was designed with a geometric scaling factor (n) of 20. Applying Iai [44] similitude principles for dimensional analysis, the derived prototype-scale parameters were calculated and are presented in Table 2.

Table 2. Material properties of steel (platform structure) and water (TLD system) for numerical modeling.

Parameter	Iai Coefficient
Horizontal Length	N
Vertical Length	N
Special Mass	1
Stress	N

Fig. 3. Experimental setup for axial load testing.

3.4. Instrumentation and micropile configuration

Given the challenges associated with load cell and linear variable differential transformer (LVDT) installation on small-diameter micropiles, a steel interface plate was implemented between the micropile head and load cell. To facilitate this configuration, micropiles were extended approximately 5 cm above the sand surface. Fig. 3 illustrates a typical loaded micropile configuration.

3.5. Grout penetration characteristics

The granular nature of the sand matrix prevented significant grout infiltration, resulting in final micropile diameters exceeding the original pipe dimensions by precisely 2 mm in all test specimens.

Fig. 4. Micropile specimens retrieved after bearing capacity testing.

3.6. Reinforcement design and performance verification

Given the study's focus on assessing the geotechnical bearing capacity of micropiles under excess pore water pressure conditions, structural reinforcement was implemented to prevent premature failure. A 2 mm diameter steel wire was incorporated into the micropile design to maintain structural integrity during testing. Post-test examination of extracted micropiles (Fig. 4) confirms the effectiveness of this reinforcement strategy, with visual inspection revealing no instances of structural failure. The specimens exhibited pure geotechnical failure modes, as evidenced by their intact condition following load testing.

3.7. Axial load testing of micropiles

Following sample preparation, the micropiles were subjected to axial loading until reaching their ultimate bearing capacity, with simultaneous recording of load-displacement measurements. To ensure adequate cement grout strength development, all load tests were performed after a 7-day curing period. The complete test matrix and results are summarized in Table 3.

Table 3. Summary of axial load test results on micropiles.

Test	Diameter (mm)	Length (mm)	r_u
R00D08	8	500	0
R05D08	8	500	0.5
R07D08	8	500	0.7
R10D08	8	500	1
R00D10	10	500	0
R05D10	10	500	0.5
R07D10	10	500	0.7
R10D10	10	500	1
R00D12	12	500	0
R05D12	12	500	0.5
R07D12	12	500	0.7
R10D12	12	500	1

3.8. Micropile performance under partial liquefaction conditions

While complete liquefaction may not develop in loose saturated sands during seismic loading, the generation of excess pore water pressure remains a critical concern. These pressure accumulations significantly degrade both the bearing capacity and stiffness of the soil matrix, often precipitating substantial settlements. Consequently, understanding sandy soil behavior under elevated pore water pressure conditions before full liquefaction is paramount. This experimental investigation systematically evaluated single micropile performance across a spectrum of pore water pressure ratios (r_u = 0, 0.5, 0.7, and 1) for micropile diameters of 8, 10, and 12 mm. The comprehensive assessment focused on both bearing capacity evolution and settlement characteristics.

Fig. 5 illustrates representative test results under a pore water pressure ratio of 0.5 for varying micropile diameters. The data reveals three critical findings:

1. All specimens exhibited comparable initial stiffness regardless of diameter.
2. Ultimate load capacity demonstrated direct proportionality with micropile diameter (10-14 mm range), increasing approximately per the enlarged side surface area (diameter + 2 mm).
3. The larger diameter micropiles induced additional tip compaction in the loose sand, enhancing resistance at greater displacements.

This dual mechanism - combining increased side friction and improved tip resistance - fundamentally alters the shear deformation pattern, manifesting in load-displacement curves that approach their asymptotes more gradually.

Fig. 6 illustrates the load-displacement response of a 10 mm diameter micropile under varying excess pore water pressure ratios (r_u = 0, 0.5, 0.7, and 1). The results demonstrate a pronounced degradation in bearing capacity with increasing pore pressure, with ultimate loads decreasing from 0.5 kN (r_u = 0) to 0.27 kN (r_u = 0.5), 0.16 kN (r_u = 0.7), and 0.11 kN (r_u = 1), representing a 78% reduction under full liquefaction conditions. Notably, while the load-displacement curves approach an asymptote under elevated pore pressures ($r_u \geq 0.7$), the behavior differs significantly in non-liquefied conditions (r_u = 0), where tip compaction enables continued load resistance at larger displacements. This suggests a fundamental shift in failure mechanisms - from sliding behavior in liquefied sand to a more ductile response characterized by progressive tip compaction in non-liquefied conditions. Although the bearing capacity decreases approximately five-fold under complete liquefaction, the residual capacity remains non-negligible (0.11 kN), a finding with important implications for post-seismic performance that is typically overlooked in conventional design practice.

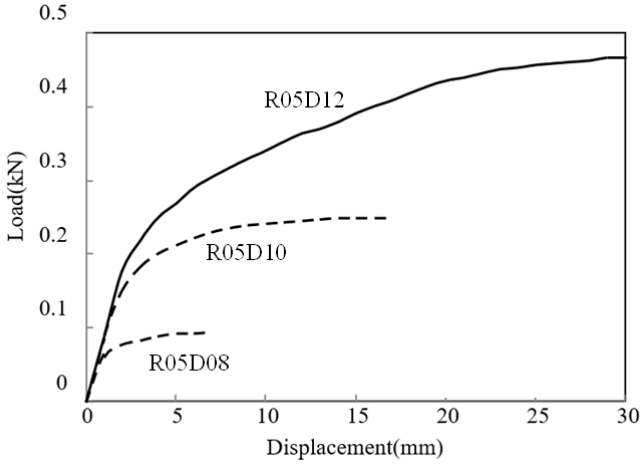

Fig. 5. Load-displacement behavior of micropiles (8, 10, and 12 mm diameters) under partial liquefaction conditions (r_u = 0.5).

The results further reveal that the capacity reduction is non-linear with respect to pore pressure increase, with the most significant degradation occurring between r_u = 0.5 and r_u = 0.7.

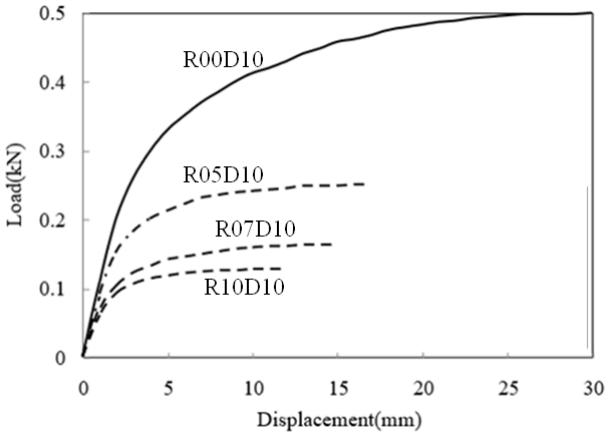

Fig. 6. Load-displacement behavior of 10 mm diameter micropile under different pore pressure ratios.

3.9. Micropiles as a liquefaction mitigation technique

Micropiles represent a relatively novel approach for liquefaction risk mitigation. While complete liquefaction may not always develop during seismic events, the generation of excess pore water pressure remains a significant concern. Consequently, assessing micropile bearing capacity and settlement behavior under moderately elevated pore pressure conditions is critically important for seismic design applications.

4. Experimental methodology

This investigation employed physical modeling to evaluate micropile performance across varying pore water pressure ratios (r_u). Twelve comprehensive tests were conducted on Type A micropiles, characterized by gravity-fed grout installation without additional pressure application. The experimental program focused specifically on:

1. Bearing capacity degradation under progressive pore pressure increase
2. Settlement accumulation patterns
3. Failure mode transitions

Consistent with industry standards FHWA [47], micropiles are categorized into four primary types (A-D) based on construction methodology and grouting technique. The current study specifically examines Type A micropiles where:

1. Grout placement occurs under gravitational force only
2. No post-grouting pressure is applied
3. Reinforcement is typically minimal

4.1. Degradation of micropile bearing capacity under increasing pore pressure ratios

Experimental results demonstrate a systematic reduction in micropile bearing capacity with increasing pore water pressure, revealing several key behavioral patterns. As shown in Fig. 7, bearing capacity decreases linearly with rising (r_u), with specimens of all diameters (8-12 mm) converging to similar performance at (r_u) > ≥ 0.7. Notably, a significant capacity reduction occurs beyond (r_u) >= 0.6, corresponding to the liquefaction initiation threshold identified by Yoshimi and Tokimatsu [4] , where soil stiffness and strength undergo marked deterioration. Larger diameter micropiles exhibit more pronounced capacity loss (35-42% at (r_u)> > 0.6 versus 28-32% for smaller diameters), attributed to the breakdown of tip compaction mechanisms under reduced effective stresses. This leads to a fundamental transition in failure modes - while larger diameters at low (r_u) (<0.5) develop asymptotic load-displacement curves through progressive tip compaction, all specimens at higher (r_u) and smaller diameters exhibit catastrophic sliding failure. Despite substantial capacity reduction (up to 78% at full liquefaction), residual load-bearing capability remains non-negligible, suggesting potential for group configurations to enhance performance through composite action (15-25% capacity increase) and confinement effects (additional 10-15%). The observed diameter-dependent behavior underscores the importance of considering both initial capacity requirements and anticipated pore pressure development in seismic design applications.

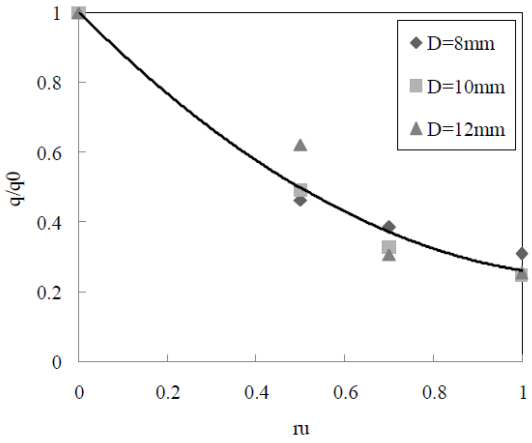

Fig. 7. Relationship between pore pressure ratio (r_u) and normalized bearing capacity for micropiles of different diameters (8, 10, and 12 mm).

4.2. Role of grout-soil cohesion in micropile design

Micropile design is predominantly governed by shaft resistance due to the substantial surface area of the grout-soil interface, which typically exceeds the tip area by a factor of 15–20, necessitating significant displacement to mobilize tip resistance. Consequently, conventional design approaches assume load transfer occurs primarily through side friction, with tip resistance often neglected [47]. The grout-soil adhesion strength thus becomes the critical parameter in capacity estimation, though current design practice remains largely empirical, relying on extrapolations from pile, soil nailing, and anchor theories. While various codes and guidelines (e.g., FHWA [47], Eurocode 7 [56]) provide empirical adhesion values for use in analytical formulations (e.g., Eq. 3), these methods often overlook key factors such as strain-dependent adhesion mobilization, construction effects (e.g., grouting pressure variations), and time-dependent strength development, highlighting the need for more refined, micropile-specific design methodologies.

$$P_{allowable} = \pi \frac{\alpha_{bondstrength}}{F.S.} D_{bond}\, L \tag{3}$$

where:

- $P_{allowable}$: allowable bearing capacity of micropile,
- $\alpha_{bond\ strength}$: grout and sand adhesion,
- $F.S.$: factor of safety,
- D_{bond}: increased diameter of micropile,
- L: length of micropile.

Fig. 8 shows Progressive degradation of grout-sand interface shear strength with increasing pore pressure ratio (r_u) in 8 mm diameter micropiles, as derived from bearing capacity measurements via Eq. 3. The experimental results demonstrate a nonlinear reduction in interfacial shear resistance, where the degradation rate decreases nonlinearly with rising (r_u) values. This behavior primarily stems from the progressive deterioration of the sand's friction angle ($\Delta\phi \approx 15$-$25°$ at $r_u = 1.0$), though notably, a residual strength component persists even under complete liquefaction conditions ($r_u = 1.0$). This residual capacity, maintained through liquefaction-induced residual resistance and a preserved minimum friction angle ($\phi > \approx 5$-$8°$), highlights the complex particulate interactions at the grout-sand interface.

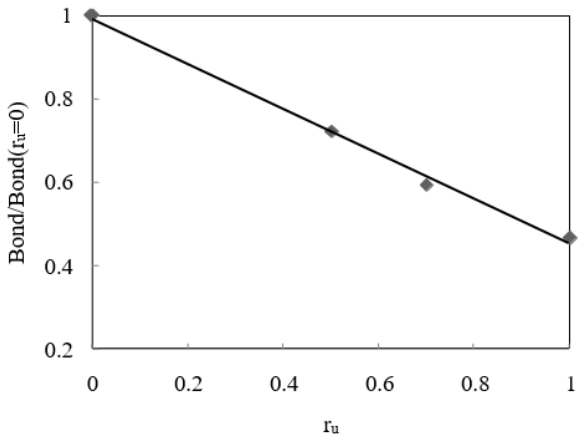

Fig. 8. The relationship between grout and sand adhesion and excess pore water pressure.

While the conventional term "adhesion" is adopted here to describe this apparent shear resistance, it should be interpreted as an operational concept for micropile design calculations rather than a strict mechanical characterization, given the fundamental differences between granular media behavior and classical adhesion mechanisms in cohesive soils. The findings underscore the need for micromechanical interpretation of interface behavior while providing practical parameters for engineering design.

The observed reduction in shaft resistance results principally from the progressive decrease in the sand's friction angle ($\Delta\phi$) as the pore pressure ratio (r_u) increases. Even under complete liquefaction conditions (r_u = 1), a measurable interface resistance persists, attributable to two key factors: (1) liquefaction-induced residual resistance, and (2) the preservation of a residual friction angle ($\phi >\approx$ 5-8°).

4.3. Pore pressure-induced settlement behavior

The generation of excess pore water pressure induces two critical geotechnical effects: (1) substantial reduction in soil stiffness and (2) potential loss of bearing capacity. While structural stability may be maintained in cases of partial liquefaction ($0.5 < r_u <$ 1.0), the associated differential settlements often exceed serviceability limits, rendering superstructures non-functional. This necessitates rigorous evaluation of liquefaction-related settlements, even before complete bearing capacity failure occurs. The fundamental design challenge lies in establishing appropriate safety factors for settlement control, particularly given the divergence among international codes (e.g., Eurocode 7 [56] recommends FS = 1.5-2.0 for serviceability, while AASHTO specifies FS ≥ 2.5 for critical infrastructure). Fig. 9 presents the correlation between dimensionless deviatoric settlements (Eq. 4) and safety factors across the pore pressure ratio spectrum, revealing three key behavioral regimes:

$$\delta = \frac{\delta_{static} - \delta_{ru}}{D} \quad (4)$$

where:

- δ: dimensionless deviatoric settlements,
- δ_{static}: settlements due to pile loading up to the intended safety factor not under r_u,
- δ_{ru}: settlements due to r_u,
- D: micropile diameter

The evaluation of liquefaction-induced settlements was performed by comparing load-settlement curves at different pore pressure ratios (r_u >= 0, 0.3, 0.5, and 1.0). As shown in Fig. 9, deviatoric settlements remain nearly constant for safety factors (FS) below 5, regardless of r_u, but exhibit progressive nonlinear growth at higher FS values, eventually approaching an asymptotic limit. Notably, higher r_u values lead to significantly larger deviatoric settlements, with the rate of accumulation increasing by approximately 40–60% per 0.2 increment in r_u. The asymptotic behavior, where settlements stabilize at maximum values, occurs at lower FS thresholds as r_u increases. These findings, derived from dimensionless settlement analysis (normalized by micropile diameter or characteristic length), highlight the critical influence of pore pressure on settlement accumulation and provide a basis for assessing serviceability limits in liquefaction-prone environments, where conventional bearing capacity factors may not adequately account for deformation-controlled failure mechanisms.

Fig. 9 shows three fundamental characteristics of pore pressure-induced settlements: (1) Below a critical safety factor (FS < 5), deviatoric settlements remain essentially invariant across all pore pressure ratios (r_u); (2) Beyond this threshold (FS ≥ 5), exhibits progressive nonlinear growth, asymptotically approaching maximum values that are strongly dependent on r_u; and (3) The magnitude of deviatoric settlements demonstrates direct correlation with increasing r_u, with settlement rates amplifying by approximately 40-60% per 0.2 r_u increment. This behavior reflects the transition from frictional resistance dominance at low r_u to particulate suspension response at elevated pore pressures, where the asymptotic stabilization occurs at progressively lower FS values as r_u increases.

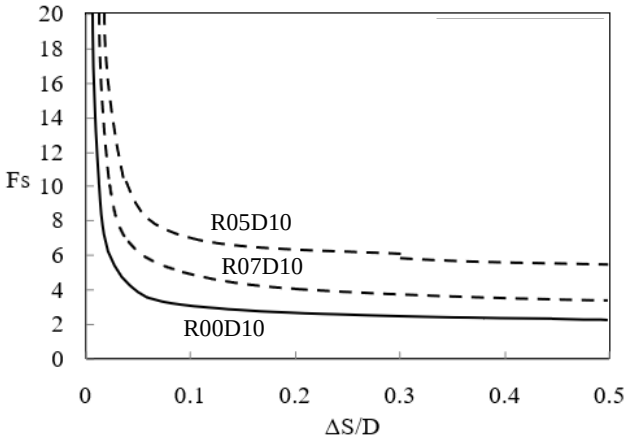

Fig. 9. Correlation between factor of safety (FS) and normalized deviatoric settlements under different pore pressure ratios.

5. Conclusions

This experimental study investigated the bearing capacity and settlement behavior of single micropiles under varying pore pressure ratios (r_u) through a series of 12 physical model tests. The results demonstrate significant degradation in micropile performance with increasing pore pressure, particularly beyond the critical threshold of $r_u > 0.6$, which corresponds to the initiation of liquefaction in granular soils. At this stage, the bearing capacity undergoes a rapid reduction due to the substantial decrease in effective stress and soil stiffness. However, even under complete liquefaction conditions ($r_u = 1.0$), a residual capacity of 15–20% of the initial value persists, attributed to the remaining shear resistance at the grout-soil interface and particulate interlocking effects. The study further reveals that micropile diameter plays a crucial role in load-bearing behavior. Larger diameters (10–12 mm) exhibit increased capacity proportional to their side surface area (πD + 2 mm) and demonstrate strain-hardening characteristics at lower ($r_u < 0.5$), owing to enhanced tip resistance and soil densification. Conversely, as r_u increases, the grout-soil adhesion coefficient (α) decreases nonlinearly, transitioning from frictional resistance at moderate pore pressures (r_u = 0–0.7) to cementation-dominated behavior under near-liquefaction conditions ($r_u > 0.7$). From a serviceability perspective, deviatoric settlements remain negligible (δ/D < 0.5%) for safety factors (FS) below 5, regardless of pore pressure conditions. However, beyond this threshold (FS ≥ 5), settlements increase nonlinearly, with higher r_u.

6. Future work

While the present study provides valuable experimental insights into the performance of micropiles under varying pore pressure ratios in liquefiable sands, several directions remain for future exploration:

- Full-scale field validation: Although the shaking table experiments yielded critical findings, translating these results to field-scale conditions requires further in-situ studies. Factors such as soil profile heterogeneity, variability in groundwater conditions, and construction effects can significantly impact micropile performance.
- Integration of numerical and machine learning approaches: Advanced computational techniques, including 3D numerical modeling and data-driven machine learning methods [57], offer significant potential for enhancing prediction accuracy. Machine learning algorithms can be trained on experimental and field data to identify hidden correlations between soil parameters, micropile geometry, and seismic responses, leading to more robust and site-specific design guidelines.
- Optimization of micropile group configurations: The current study focused primarily on single micropiles. Future research should investigate the interaction effects of micropile groups under seismic conditions. Machine learning optimization frameworks could be employed to determine optimal spacing, inclination, and reinforcement configurations that maximize bearing capacity while minimizing settlements.
- Long-term performance under cyclic loading: Seismic loading often includes multiple cycles with varying amplitudes. Future studies should examine the cumulative degradation of micropile capacity under prolonged cyclic loading and assess resilience during aftershocks.

Statements & Declarations

Author contributions

Mohammad Ali. Arjomand: Conceptualization, Formal analysis, Investigation, Methodology, Supervision, Visualization, Writing - Review & Editing.

Mohsen Bagheri: Data curation, Formal analysis, Investigation, Methodology, Supervision, Visualization, Writing - Review & Editing.

Yashar Mostafaei: Conceptualization, Resources, Writing - Original Draft.

Hosein Mola-Abasi: Conceptualization, Formal analysis, Investigation, Methodology, Supervision, Visualization, Writing - Review & Editing.

Funding

The authors declare that no funds, grants, or other support were received during the preparation of this manuscript.

Data availability

The datasets analyzed in the current study are available from the corresponding author on reasonable request. Declarations The authors declare no conflict of interest.

References

[1] Kawakami, F., Asada, A. Damage to the ground and earth structures by the Niigata earthquake of June 16, 1964. Soils and Foundations, 1966; 6: 14-30. doi:10.3208/sandf1960.6.14.

[2] Kishida, H. Damage to reinforced concrete buildings in Niigata city with special reference to foundation engineering. Soils and Foundations, 1966; 6: 71-88. doi:10.3208/sandf1960.6.71.

[3] Ohsaki, Y. Niigata earthquakes, 1964 building damage and soil condition. Soils and Foundations, 1966; 6: 14-37. doi:10.3208/sandf1960.6.2_14.

[4] Yoshimi, Y., Tokimatsu, K. Settlement of buildings on saturated sand during earthquakes. Soils and Foundations, 1977; 17: 23-38. doi:10.3208/sandf1972.17.23.

[5] Nagase, H., Ishihara, K. Liquefaction-induced compaction and settlement of sand during earthquakes. Soils and Foundations, 1988; 28: 65-76. doi:10.3208/sandf1972.28.65.

[6] Seed, H. B., Idriss, I. M. Analysis of soil liquefaction: Niigata earthquake. Journal of the Soil Mechanics and Foundations Division, 1967; 93: 83-108. doi:10.1061/JSFEAQ.0000981.

[7] Acacio, A. A., Kobayashi, Y., Towhata, I., Bautista, R., Ishihara, K. Subsidence of building foundation resting upon liquefied subsoil: case studies and assessment. Soils and Foundations, 2001; 41: 111-128. doi:10.3208/sandf.41.6_111.

[8] Ishihara, K., Acacio, A. A., Towhata, I. Liquefaction-induced ground damage in Dagupan in the July 16, 1990 Luzon earthquake. Soils and Foundations, 1993; 33: 133-154. doi:10.3208/sandf1972.33.133.

[9] Tokimatsu, K., Kojima, H., Kuwayama, S., Abe, A., Midorikawa, S. Liquefaction-induced damage to buildings in 1990 Luzon earthquake. Journal of Geotechnical Engineering, 1994; 120: 290-307. doi:10.1061/(ASCE)0733-9410(1994)120:2(290).

[10] Yasui, M. Settlement and inclination of reinforced concrete buildings in Dagupan City due to liquefaction during the 1990 Philippine earthquake. In: The 10th World Conference on Earthquake Engineering; 1992 Jul 19-24; Madrid, Spain. p. 147-152.

[11] Bray, J. D., Sancio, R. B., Durgunoglu, T., Onalp, A., Youd, T. L., Stewart, J. P., Seed, R. B., Cetin, O. K., Bol, E., Baturay, M. B. Subsurface characterization at ground failure sites in Adapazari, Turkey. Journal of geotechnical and geoenvironmental engineering, 2004; 130: 673-685. doi:10.1061/(ASCE)1090-0241(2004)130:7(673).

[12] Sancio, R., Bray, J. D., Durgunoglu, T., Onalp, A. Performance of buildings over liquefiable ground in Adapazari, Turkey. In: The 13th World Conference on Earthquake Engineering; 2004 Aug 1-6; Vancouver, Canada. p. 1-15.

[13] Yoshida, N., Tokimatsu, K., Yasuda, S., Kokusho, T., Okimura, T. Geotechnical aspects of damage in Adapazari city during 1999 Kocaeli, Turkey earthquake. Soils and Foundations, 2001; 41: 25-45. doi:10.3208/sandf.41.4_25.

[14] Coelho, P., Haigh, S., Madabhushi, S. Centrifuge modelling of liquefaction of saturated sand under cyclic loading. In: Proceedings of the international conference on cyclic behaviour of soils and liquefaction phenomena; 2004 Mar 31-Apr 2; Bochum, Germany. p. 349-354.

[15] Coelho, P., Haigh, S. K., Madabhushi, S. G., O'Brien, T. Centrifuge modeling of the use of densification as a liquefaction resistance measure for bridge foundations. In: The 13th World Conference on Earthquake Engineering; 2004 Aug 1–6; Vancouver, Canada. p. 210-225.

[16] Dashti, S., Bray, J. D., Pestana, J. M., Riemer, M., Wilson, D. Mechanisms of seismically induced settlement of buildings with shallow foundations on liquefiable soil. Journal of geotechnical and geoenvironmental engineering, 2010; 136: 151-164. doi:10.1061/(ASCE)GT.1943-5606.0000179.

[17] Dashti, S., Bray, J. D., Pestana, J. M., Riemer, M., Wilson, D. Centrifuge testing to evaluate and mitigate liquefaction-induced building settlement mechanisms. Journal of geotechnical and geoenvironmental engineering, 2010; 136: 918-929. doi:10.1061/(ASCE)GT.1943-5606.0000306.

[18] Dobry, R., Liu, L. Centrifuge modeling of soil liquefaction. In: The 10th World Conference on Earthquake Engineering; 1992 Jul 19-24; Madrid, Spain. p. 6801-6809.

[19] Liu, L. Centrifuge earthquake modelling of liquefaction and its effect on shallow foundations, (PhD Thesis). Troy (NY): Rensselaer Polytechnic Institute; 1992.

[20] Liu, L., Dobry, R. Seismic response of shallow foundation on liquefiable sand. Journal of geotechnical and geoenvironmental engineering, 1997; 123: 557-567. doi:10.1061/(ASCE)1090-0241(1997)123:6(557).

[21] Liu, L., Dobry, R. Centrifuge study of shallow foundation on saturated sand during earthquakes. In: Proceedings from the fourth Japan-US workshop on earthquake resistant design of lifeline facilities and countermeasures for soil liquefaction; 1992 May 27-29; Honolulu, United States. p. 493-508.

[22] Ueng, T., Wu, C., Cheng, H., Chen, C. Settlements of saturated clean sand deposits in shaking table tests. Soil Dynamics and Earthquake Engineering, 2010; 30: 50-60. doi:10.1016/j.soildyn.2009.09.006.

[23] Adalier, K., Elgamal, A. Mitigation of liquefaction and associated ground deformations by stone columns. Engineering Geology, 2004; 72: 275-291. doi:10.1016/j.enggeo.2003.11.001.

[24] Adalier, K., Elgamal, A., Meneses, J., Baez, J. Stone columns as liquefaction countermeasure in non-plastic silty soils. Soil Dynamics and Earthquake Engineering, 2003; 23: 571-584. doi:10.1016/S0267-7261(03)00070-8.

[25] Asgari, A., Oliaei, M., Bagheri, M. Numerical simulation of improvement of a liquefiable soil layer using stone column and pile-pinning techniques. Soil Dynamics and Earthquake Engineering, 2013; 51: 77-96. doi:10.1016/j.soildyn.2013.04.006.

[26] Burcharth, H. F. Breakwaters with vertical and inclined concrete walls: Report of working group 28 of the maritime navigation commission. ed. Brussels (BE): PIANC General Secretariat; 2003.

[27] Lu, J., Elgamal, A., Yan, L., Law, K. H., Conte, J. P. Large-scale numerical modeling in geotechnical earthquake engineering. International Journal of Geomechanics, 2011; 11: 490-503. doi:10.1061/(ASCE)GM.1943-5622.0000042.

[28] Kuwano, J., Takahashi, A., Nakada, T., Yano, A., Kido, M. Centrifuge model loading tests on slope stabilizing micro-piles. In: Advances in geotechnical engineering: The Skempton conference: Proceedings of a three day conference on advances in geotechnical engineering; 2004 Mar 29-31; London, UK. p. 1080-1089.

[29] Nusier, O., Alawneh, A., Rabadi, R. Micropiles reinforcement for expansive soils: large-scale experimental investigation. Proceedings of the Institution of Civil Engineers-Ground Improvement, 2007; 11: 55-60. doi:10.1680/grim.2007.11.2.55.

[30] Nusier, O. K., Alawneh, A. S., Abdullatit, B. Small-scale micropiles to control heave on expansive clays. Proceedings of the Institution of Civil Engineers-Ground Improvement, 2009; 162: 27-35. doi:10.1680/grim.2009.162.1.27.

[31] Srinivasa Murthy, B., Sivakumar Babu, G., Srinivas, A. Analysis of bearing capacity improvement using micropiles. Proceedings of the Institution of Civil Engineers-Ground Improvement, 2002; 6: 121-128. doi:10.1680/grim.2002.6.3.121.

[32] Asgari, A., Bagheri, M., Hadizadeh, M. Advanced seismic analysis of soil-foundation-structure interaction for shallow and pile foundations in saturated and dry deposits: Insights from 3D parallel finite element modeling. Structures, 2024; 69: 107503. doi:10.1016/j.istruc.2024.107503.

[33] Wang, M., Han, J. Numerical Modelling for Ground Improvement of Batter Micropiles on Liquefiable Soils. In: A. J. Puppala, J. Huang, J. Han, L. R. Hoyos editors. Ground Improvement and Geosynthetics. 2012. p. 212-219. doi:10.1061/41108(381)28.

[34] Ghassemi, S., Ekraminia, S. S., Hajialilue-Bonab, M., Tohidvand, H. R., Azarafza, M., Derakhshani, R. Innovative insights into micropile seismic response: Shaking table tests reveal critical dependencies and liquefaction mitigation. Bulletin of Engineering Geology and the Environment, 2025; 84: 206. doi:10.1007/s10064-025-04225-y.

[35] Jalilian, H., Yin, J. H., Panah, A. K. Shaking Table Investigation of Seismic Performance of Micropiles. In: Proceedings of GeoShanghai 2018 International Conference: Advances in Soil Dynamics and Foundation Engineering; 2018; Singapore. p. 138-147. doi:10.1007/978-981-13-0131-5_16.

[36] Shahrour, I., Juran, I. Seismic behaviour of micropile systems. Proceedings of the Institution of Civil Engineers-Ground Improvement, 2004; 8: 109-120.

[37] Capatti, M. C., Dezi, F., Carbonari, S., Gara, F. Full-scale experimental assessment of the dynamic horizontal behavior of micropiles in alluvial silty soils. Soil Dynamics and Earthquake Engineering, 2018; 113: 58-74. doi:10.1016/j.soildyn.2018.05.029.

[38] Capatti, M. C., Dezi, F., Carbonari, S., Gara, F. Dynamic performance of a full-scale micropile group: Relevance of nonlinear behaviour of the soil adjacent to micropiles. Soil Dynamics and Earthquake Engineering, 2020; 128: 105858. doi:10.1016/j.soildyn.2019.105858.

[39] Jalilian Mashhoud, H., Yin, J.-H., Komak Panah, A., Leung, Y. F. Shaking table test study on dynamic behavior of micropiles in loose sand. Soil Dynamics and Earthquake Engineering, 2018; 110: 53-69. doi:10.1016/j.soildyn.2018.03.008.

[40] Alnuaim, A. M., El Naggar, M. H., El Naggar, H. Numerical investigation of the performance of micropiled rafts in sand. Computers and Geotechnics, 2016; 77: 91-105. doi:10.1016/j.compgeo.2016.04.002.

[41] Asgari, A., Arjomand, M. A., Bagheri, M., Ebadi-Jamkhaneh, M., Mostafaei, Y. Assessment of Experimental Data and Analytical Method of Helical Pile Capacity Under Tension and Compressive Loading in Dense Sand. Buildings, 2025; 15: 2683. doi:10.3390/buildings15152683.

[42] Barari, A., Bagheri, M., Rouainia, M., Ibsen, L. B. Deformation mechanisms for offshore monopile foundations accounting for cyclic mobility effects. Soil Dynamics and Earthquake Engineering, 2017; 97: 439-453. doi:10.1016/j.soildyn.2017.03.008.

[43] Vargas, W. Ring shear tests on large deformation of sand, (PhD Thesis). Tokyo (JP): The University of Tokyo; 1998.

[44] Iai, S. Similitude for shaking table tests on soil-structure-fluid model in 1g gravitational field. Soils and Foundations, 1989; 29: 105-118. doi:10.3208/sandf1972.29.105.

[45] Kagawa, T. On the similitude in model vibration tests of earth-structures. Proceedings of the Japan Society of Civil Engineers, 1978; 1978: 69-77. doi:10.2208/jscej1969.1978.275_69.

[46] Kokusho, T., Iwatate, T. Scaled model tests and numerical analyses on nonlinear dynamic response of soft grounds. Proceedings of the Japan Society of Civil Engineers, 1979; 1979: 57-67. doi:10.2208/jscej1969.1979.285_57.

[47] Federal Highway Administration (FHWA). FHWA-SA-97-070: FHWA, Micropile design and construction guidlines. United States Department of Transportation Federal Highway Administration: Washington (DC); 2003.

[48] Asgari, A., Ranjbar, F., Bagheri, M. Seismic resilience of pile groups to lateral spreading in liquefiable soils: 3D parallel finite element modeling. Structures, 2025; 74: 108578. doi:10.1016/j.istruc.2025.108578.

[49] Asgari, A., Golshani, A., Bagheri, M. Numerical evaluation of seismic response of shallow foundation on loose silt and silty sand. Journal of Earth System Science, 2014; 123: 365-379. doi:10.1007/s12040-013-0393-9.

[50] Bagheri, M., Jamkhaneh, M. E., Samali, B. Effect of seismic soil–pile–structure interaction on mid-and high-rise steel buildings resting on a group of pile foundations. International Journal of Geomechanics, 2018; 18: 04018103. doi:10.1061/(ASCE)GM.1943-5622.0001222.

[51] Ibsen, L. B., Asgari, A., Bagheri, M., Barari, A. Response of monopiles in sand subjected to one-way and transient cyclic lateral loading. In: R. Y. Linag, J. Qian, J. Tao editors. Advances in Soil Dynamics and Foundation Engineering. 2014. p. 312-322. doi:10.1061/9780784413425.032.

[52] Jafarian, Y., Bagheri, M., khalili, M. Earthquake-Induced Deformation of Breakwater on Liquefiable Soil with and Without Remediation: Case Study of Iran LNG Port. In: New Developments in Materials for Infrastructure Sustainability and the Contemporary Issues in Geo-environmental Engineering; 2019; Cham, Switzerland. p. 23-37. doi:10.1007/978-3-319-95774-6_3.

[53] Patrício, J. D., Gusmão, A. D., Ferreira, S. R., Silva, F. A., Kafshgarkolaei, H. J., Azevedo, A. C., Delgado, J. M. Settlement analysis of concrete-walled buildings using soil–structure interactions and finite element modeling. Buildings, 2024; 14: 746. doi:10.3390/buildings14030746.

[54] Shooshpasha, I., Bagheri, M. The effects of surcharge on liquefaction resistance of silty sand. Arabian Journal of Geosciences, 2014; 7: 1029-1035. doi:10.1007/s12517-012-0737-9.

[55] Asgari, A., Ahmadtabar Sorkhi, S. F. Wind turbine performance under multi-hazard loads: Wave, wind, and earthquake effects on liquefiable soil. Results in Engineering, 2025; 26: 104647. doi:10.1016/j.rineng.2025.104647.

[56] Orr, T. L., Farrell, E. R. Geotechnical design to Eurocode 7. 1st ed. Berlin (DE): Springer Science & Business Media; 2012. doi:10.1007/978-1-4471-0803-0.

[57] Jahangiri, V., Akbarzadeh, M. R., Shahamat, S. A., Asgari, A., Naeim, B., Ranjbar, F. Machine learning-based prediction of seismic response of steel diagrid systems. Structures, 2025; 80: 109791. doi:10.1016/j.istruc.2025.109791.